International Journal of Advanced Science and Technology
Vol. 29, No. 3s, (2020), pp. 1436-1453

SYNTHESIS AND STRUCTURAL CHARACTERIZATION OF UNDOPED CeO_2 AND PD DOPED CeO_2 FOR PHOTO CATALYTIC STUDIES UNDER SUNLIGHT AND UV-LIGHT IRRADIATION.

G.O. Obaiah [a, b], K.H. Shivaprasad*[a], M. Mylarappa*[c, d]
[a]*Department of chemistry, Vijayanagara Sri Krishna Devaraya University, Ballary -583104, Karnataka, India*
[b]*Research centre, Talent development centre, IISC, Kudhapur, Chitradurga-577501, Karnataka, India*
Department of chemistry, Sri Jagadguru Renukacharya College of Science, Arts & Commerce, Race course Road Bengaluru-560009, Karnataka, India
Corresponding Author

Abstract

The main objective of the analysis is concentrated on the preparation and fabrication of doped and undoped CeO_2 nanoparticles by solution combustion technique to taken glycine as fuel. The correct size and morphology of the doped metal compounds were studied Scanning microscope (SEM). The composition of ceria (CeO_2) and palladium substituted Ceria ($Ce_{0.98}Pd_{0.02}O_2$) was confirmed from the powder X-ray Diffractometer (PXRD). The functional groups were analyzed by Fourier transfer infrared spectroscopic analysis, XRD, RR, UV–Vis, and XPS. Photocatalytic properties of CeO_2 and palladium doped CeO_2 ($Ce_{0.98}Pd_{0.02}O_2$) nanoparticles (NPs) were studied using the radiation conjugation of red (CR) under UV light and sunlight exposure. Based on the XRD analysis, CeO_2 and Pd doped CeO_2 NPs were formed as crystal structures. CeO_2 and Pd doped CeO_2 showed excellent Photocatalytic activity by degrading more than 92% of the CR color in the intervals of 120 min under UV light and sunlight.

Keywords: *$PdCl_2$; $(NH_4)_2Ce(NO_3)_6$. NH_2CH_2COOH,CeO_2, $Ce_{0.98}Pd_{0.02}O_2$, Congo red.*

1. Introduction

In the current study, we can develop a regular solid catalyst wherever the catalyst may be a unique phage solid having a definite structural and its potential to distinguish the active area of the catalysts for the chemical process. The palladium metallic element is the least expensive and most typically used metal. CeO_2 absorbs lightweight within the close to ultraviolet radiation and small light within the visible region. Further, Cerium dioxide (CeO_2) composite materials were used as a cost-effective, chemical change catalyst, economical chemical reaction catalysts, distinctive oxidation-reduction property, oxygen storage capability (OSC), environmental catalysts for natural and synthetic process to pull down of assorted volatile organic compounds to the removal of contaminates from carbon dioxide [1-3].

Palladium based catalysts significantly nanoscale metallic element particles have recently drawn massive attention because of their versatile role in organic synthesis [4-5]. The employment of Pd in catalysis not only in industrial [4-6] but also the catalytic activity, size, shape, form, yet as the nature of close to the surrounding media [7]. CeO_2 has been wide investigated as support in three-parts of catalysts for exhaust gas treatment from vehicles [8-9], water gas shift catalysts [10-11], electro-oxidation catalyst [12], oxygen particle in a compound fuel cells [13], sprucing chemical, mechanical and planarization technique [14], the molecular, structural compounds of semiconductor devices [15], ultraviolet difficulty materials [16].

Metal oxides became the most productive palladium supports for heterogeneous catalytic chemical change action due to their accessibility, low production costs, and photo induction hole pairs on the surfaces of a metal compound that could be harvested to spice up electron transfer and their chemical reactivity [31].

Newly, it has received intense attention utilizing support interactions to extend electrochemical catalytic action and the stability of supported metal catalysts [17-19]. Additionally confirmed that the

ISSN: 2005-4238 IJAST

communications could be modified with the electronic structure of the metal catalyst, that go change in chemical actions of catalytic activity, the sturdiness of the support materials may additionally influence the durability of the resultant catalyst [20]. At the low-temperature treating (350^0 to 450^0), it denotes a favorable application and CeO_2based catalyst [21-23].

The synthesis of ceria and palladium doped ceria is most useful for the high oxygen storage capability. The synthesized doped metal oxides are characterized by PXRD, SEM, Most applications of this catalyst are employed as high rates of H_2+O_2 recombination, solvent-free reduction of aromatic nitro compounds to amines as high with olefins ready [30]. CeO_2 could be nontoxic reducing oxides, and metal ions are substituted in CeO_2.In $Ce_{1-x}M_xO_{2-x}$(x= 0.01,0.02and 0.03) wherever metallic element palladium having +2 oxidation state showed high rates of nitro to amine reduction and sensible picture chemical change activity for CO reaction. Smaller the metal particle, higher is that the quantity of CO absorption and better is that the chemical change conversion. Nanoparticles of high-quality metals (Pt, Pd, Rh, Ru, and Au) hold titania, alumina, and chemicals. These catalysts are often associated with natural compounds, petro chemistry [30]. The synthesis of CeO_2 nanoparticles in a variety of, and growing important because of its applications for fuel cells, solar cells, gateways for metal oxides, semiconductor devices, and phosphor [24-25]. This paper reports on the molecular characterization and characterization of CeO_2 and Pd Doped CeO_2 nanoparticles using a molecular method. Among the pollutants, pollutants such as Congo red (CR), are one of the most widely used in almost all of these industries. The destruction of red sunlight is an effective and unique method for the elimination of waste and safe water. Along with the finite element properties, the photo catalysis system using the semiconductor has attracted considerable attention since it provides environmental and economic features [32-34]. Cerium oxide (CeO_2), a Photocatalytic solvent, has attracted considerable interest from researchers because of its electrical, optical, and chemical properties [35, 36]. CeO_2 is an important component, in part due to the redox potential of the Ce^{4+} / Ce^{3+} coupler, as well as its chemical and photochemical resistance, as well as its strong light absorption in the UV region (extraction, 385-700 nm). Unfortunately, large quantities of CeO_2 [37–38] are severely restricted by large band gap (3.2 eV). Machine correction tools (e.g., TiO_2, ZnO, CeO_2, SnO_2, NiO, etc.) are of particular interest to the electronic media because of their unique electronic properties, diagnostic properties, and transmitting travel features. And porosity [39]. Usually, Photocatalytic systems use semiconductors such as TiO_2, WO_2, and ZnO as UV detectors [40-42]. Cerium oxide (CeO_2) is another active ingredient that is used in the UV light field. The efficiency of the ceria is accompanied by several advantages such as its high band gap (3.2-eV) [43], high sensitivity [44], high-frequency domain [45], potential high oxygen concentration [44] and the ability to respond [45]. Among heterogeneous photocatalysts, cerium dioxide (CeO_2) is one of its most efficient functions because of its efficacy in damaging the water and water. However, the narrow band of CeO_2 (3.0–3.4 eV) has been restricted to Photocatalytic activity by the photo excited electron/ion coupler during light irradiation [46–48]. It is important to prevent this process from the use of metal ions, which can produce impurities in the CeO_2 group configuration for car compensation and reduce the redox bond rate as well as facilitate the redox reaction on the surface of the photocatalysts. [49-51]. Palladium ion-based ionization as a potential catalyst for Pd^{2+}/Pd^{3+} and Pd^{+} / Pd^{2+} levels, which can act as a low-energy ion for electron or hole-based catalysts. the position of Fermi level is present. and where they live. [52]. The work was intended to convert CeO_2 fibers using Pd ion using different percentages (0.5, 1.0, 1.5, and 2.0 wt%) to perform the same methods as water, impregnation, and calcination methods. The use of XPS, XRD, FESEM / EDS, spectroscopy, spectroscopy, and CeO_2 spectroscopy due to the Pd dopant were studied by experimental data, spectroscopy, and IR measurements. Sampling, the development of highly visible, non-toxic, and chemical compounds under long-light emission. Semiconductor provides support such as SnO_2 (Sangaami and Dhaarmaraj, 2013), CeO_2 (Yongchuan et al., 2014), chalcogenides metal. The activity of Pd on CeO_2 for both un-doped ceria and palladium doped ceria materials were analyzed in terms of lattice parameters, average crystalline size, and small internal strains. Within the present work, CeO_2 and palladium doped CeO_2 ($Ce_{0.98}Pd_{0.02}O_2$)nanoparticles were prepared by solution combustion methodology, glycine as

ISSN: 2005-4238 IJAST

fuel and the final product was well characterized by PXRD, Scanning microscopy, Rietveld refinement method(RRM), Fourier transformation of infrared spectrum analysis (FT-IR), Ultraviolet-visible spectrum analysis (UV).

2. Experimental method

2.0. Materials

Ceric ammonium nitrate $(NH_4)_2Ce\ (NO_3)_6$, Glycine NH_2CH_2COOH, and metallic element Palladium chloride $PdCl_2$ was purchased from Merck. The combustion technique prepared ceria (CeO2) and Pd-doped ceria catalysts, Congo red.

2.1. Synthesis of Cerium dioxide (CeO_2) nanoparticles

The starting materials area $(NH_4)_2Ce(NO_3)_6$, and glycine as fuel. For the synthesis of CeO_2, the stoichiometric ratio of starting materials were to be taken as 9.89 mmol of ceric nitrate $(NH_4)_2Ce(NO_3)_6$ and 10.9 mmol of glycine in a 300ml capability crystallization salt in a container, the reactants were dissolved in 15 ml of water, and the solution was introduced into a preheated chamber at 350°C. The solution ignited to burn with a flame takes place once dehydration is completed to get the voluminous reliable product is obtained. The solid product was chosen for structural characterization.

$$5Ce(NH_4)_2(NO_3)_6 + 12C_2N_4H_6O_2 \rightarrow 5CeO_2 + 24CO_2 + 44N_2 + 36H_2O \ldots\ldots (1)$$

2.2. Synthesis of Palladium Doped Ceria ($Ce_{0.98}Pd_{0.02}O_2$).

The Palladium doped ceria catalyst was synthesized using the combustion method. The compound $Ce_{0.98}Pd_{0.02}O_2$ can be prepared from the solution combustion method. The starting materials are Ceric ammonium nitrate $(NH_4)_2Ce(NO_3)_6$, Palladium chloride $PdCl_2$, and glycine NH_2CH_2COOH as fuel. For the synthesis of $Ce_{0.98}Pd_{0.02}O_2$ by taking the stoichiometric ratio of beginning materials were to be taken as 9.89 mmol of Ceric ammonium nitrate $(NH_4)_2Ce(NO_3)_6$, 0.21mmol of $PdCl_2$ and 10.99 mmol of glycine in a 300ml capability of crystallization borosilicate salt container(dish). These three compounds were wholly dissolved in 25 ml H_2O, and the solution was brought in to preheated chamber at 350°C. The solution burns with flame once dehydration is completed to an obtained solid product. The reliable product was taken for the structural characterization, and we have record X-ray diffraction techniques and the Rietveld refinement method. Solution combustion synthesis for Ce1-xPdxO2 can be written as follows:

$$9(1-x)(NH_4)_2Ce(NO_3)_6 + 24(1-x)C_2H_5NO_2 + 9xPdCl_2 \rightarrow 9Ce_{1-x}Pd_xO_{2-\delta} + 96(1-x)N_2 + 48(1-x)CO_2 + (96-114x)H_2O + 18xHCl \ldots\ldots (2)$$

2.3. Evaluations of Photocatalytic activities

The photocatalytic activity of the adsorbents was investigated by the dissolution of the Rome hair filter (CR) (10 mg / L) under visible UV irradiation. All reactions were performed at room temperature with average air temperature. 60 mg of catalyst was dissolved in 100 mL shampoo. Before irradiation, the cells were placed in a dark environment, and the magnetic stirred for 30 min until they reached the adsorption-desorption level. From this, the photographic reaction began with the introduction of visible light in the system. 5mL of the solution was taken at intervals and centrifuged to remove the particles, and the results of the irradiation were determined using a UV-vis spectrophotometer. The photocatalytic activity of the reagents evaluated the interference of the seawater. The photocatalytic reaction efficiency was calculated using Equation (1).

$$\text{Resolution Capacity (DE\%)} = C_0 - C_t / C_0 \times 100 \ldots\ldots (3)$$

Where 'C_0' is the original concentration and 'C_t' or photo concentration or time constant.

2.4 Photodegradation

In the standard procedure, the concentration of photocatalyst was added to 100 mL of CR (20 ppm). The solution was stirred for 30 min in the dark to produce adsorption-desorption equilibrium between droplets

and surface. The xenon vapor pressure lamp (252 W) was used to generate visible light in the range of 450–850 nm to generate fluorescent light and chemical imaging (Lelesil Innovative System, Thane, India). The solvent was isolated from the reaction after every 15 minutes monitoring the progress of the dissolution process. The spectra were transmitted over a distance, and the UV-harmonics obtained using a UV - Vis spectrophotometer (maximum optical resolution for CR λ = 498 nm).

3. Result and discussion

3.1. PXRD (Powder X-Ray diffraction analysis)

X-ray diffraction pattern of CeO_2, palladium doped CeO_2 were recorded to X-ray diffractometer Shimadzu model: XRD 6000 with Cu Kα radiations varies 20-700 (λ=0.15nm). The XRD peaks of the CeO_2 and ($Ce_{0.98}Pd_{0.02}O_2$) nanoparticle obtain by the combustion method. The structures were characterized by PXRD, and the structure was refined by the Rietveld refinement technique, exploitation Full Prof-TB program. The Rietveld refinement methodology and, therefore, the program is employed to recognize the different phases present within the solid compound. The XRD patterns are index as anatase phase of CeO_2, and additionally, the physical phenomenon data were in good a correspondence with JCPDS Number.340394.The average crystal size was obtained by Scherrer's formula:

$$\text{Crystalline size (D)} = K\lambda/(\beta \cos\theta) \quad (4)$$

D is the size of the crystal in nm; λ is the wavelengths of the X-ray (λ=0.154 A^0in nm) for Cu Kα; K is the crystal form is 0.9, θ is the brag's angle, and β is the 0.5 high dimension at half-maximum height. The Rietveld refined patterns of CeO_2 and $Ce_{0.98}Pd_{0.02}O_2$as shown in Figure c). The profile is indexed to anatase tetragonal shape of CeO_2increases 1 to 2 atomic percentage of palladium metal may be detected by the slow scan. If the Palladium metal particle was substituted for the Ce^{4+} particle showed six coordination centers. The Rietveld refinement information was given by equation (4).

$$\beta = (Utan2\theta + Vtan\theta + W)1/2 \ldots\ldots (5)$$

Crystalline size obtained each of the strategies together. The parameter, Rf, Rbragg, $\chi 2$ area unit, summarized the below Table.1. The lattice parameter (a), of CeO_2, is 5.411 (JCPDS.No.21-1272). The lattice parameter (a) of nanocrystalline CeO_2 is slightly lower than palladium doped CeO_2 (5.411). Typical analysis of the catalysts was shown in Fig.a) that showed experimental and calculated values of powdered XRD patterns obtained by the refinement of CeO_2 and palladium doped CeO_2. The parameters (Rf, Rbragg, $\chi 2$) showed decent accordance between the Rietveld refined and determined XRD patterns for cuboids of CeO_2. The refined lattice parameter value of CeO_2 and palladium doped CeO_2 are 5.5 nm (A^0)and 3.7 nm (A^0). The cell volume of CeO_2 confirming that the cuboid structure. The powder samples were further confirmed by the refinement of the diffraction patterns with the Rietveld method. Fig.c) and d), shows the Rietveld refinement method. The improvement could be a methodology within the profile that shows the potency of scanning measurements of the particles permit to estimate an approximate structural model for the vital CeO_2 and palladium doped CeO_2 structures.

Table.1.Structural Parameter of $CeO_2$and $Ce_{0.98}Pd_{0.02}O_2$

Catalysts	Lattice parameter (a)	Rf	Rbragg	$\chi 2$	Crystalline Size (nm)	Rietveld refinement size (nm)
CeO_2	5.410(1)	0.51	0.71	1.14	5.9	5.5
$Ce_{0.98}Pd_{0.02}O_2$	5.411(1)	0.81	1.08	1.39	3.1	3.7

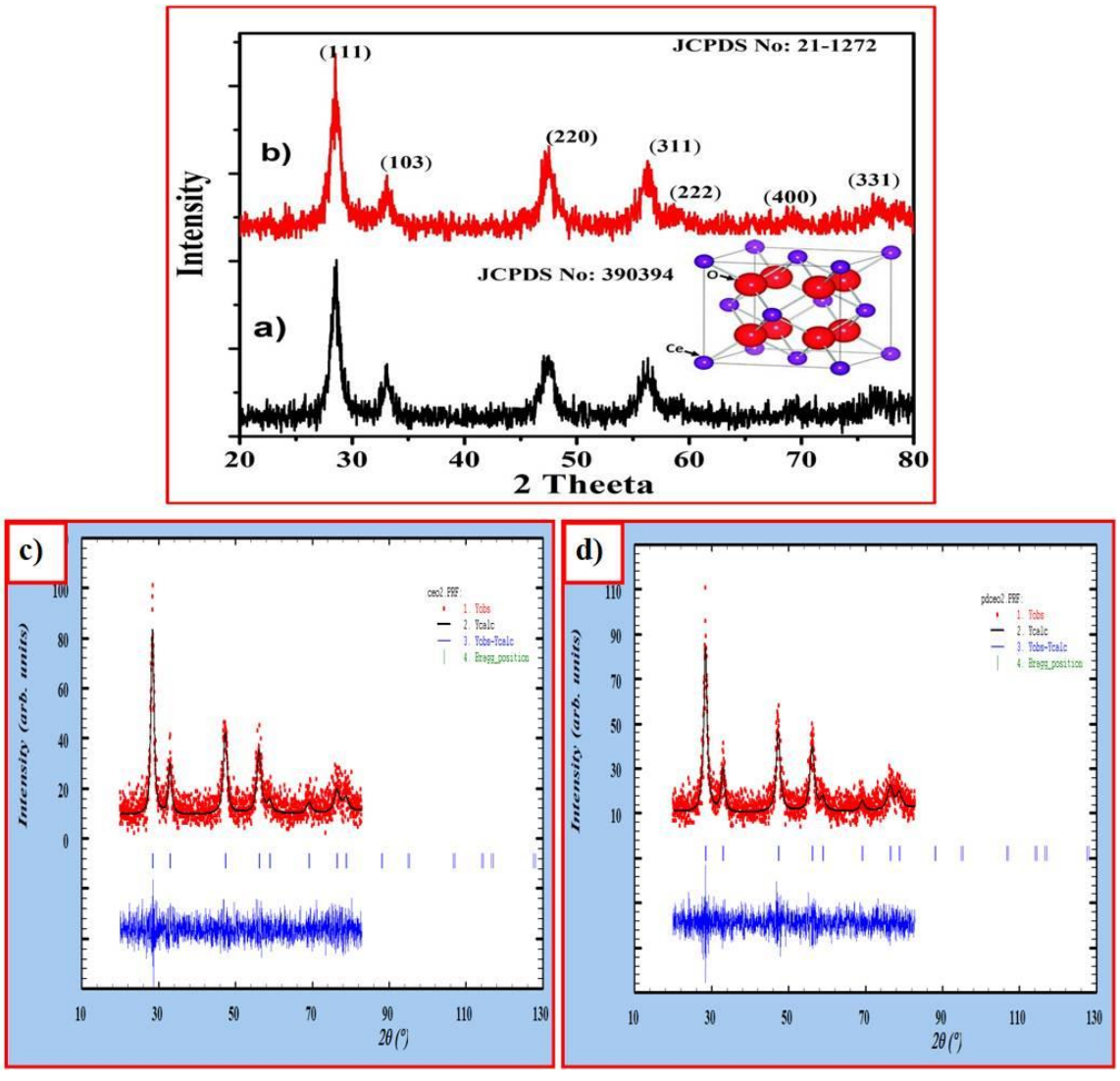

Fig 1.XRD Pattern and of Rietveld refined structures of a) CeO_2 and b) $Ce_{0.98}Pd_{0.02}O_2$ c) CeO_2 d) $Ce_{0.98}Pd_{0.02}O_2$

3.2. SEM (Scanning Electron microscopic analysis)

The Scanning electron microscopy pictures of $CeO_2$and metallic element of palladium doped CeO_2 is ready to show, the interpret nanoparticles structures additionally may be seen in grain size ~ 1μm and also two-dimensional figure showed, the evidence of the nanoparticles is very little accumulation, and a two-dimensional figure showed morphology. The SEM analysis of $Ce_{0.98}Pd_{0.02}O_2$catalyst doesn't have any impact on the morphology and structure of the CeO_2nanoparticles. The SEM analyses showed top homogeneity at time intervals, the prepared palladium doped CeO_2 samples surface area increasing the hardening temperature. These results show that the morphology of particles changes to the spherical kind with less quantity by increasing temperature. The SEM analysis of the typical crystal size of tempered nanocrystals is regarding ~ 20nm.

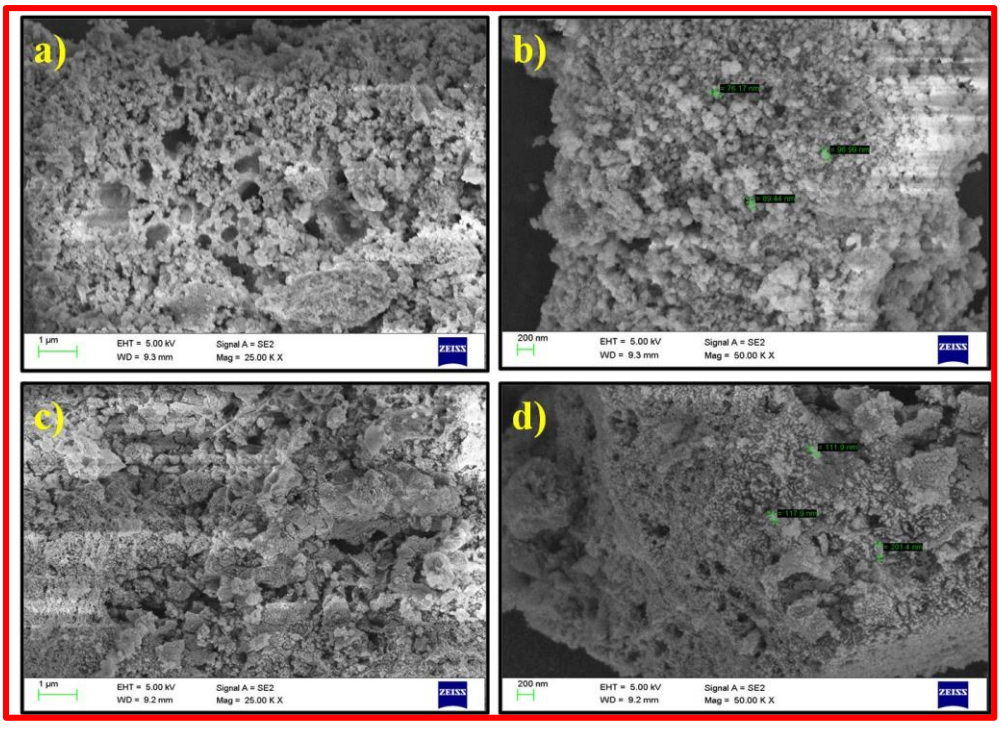

Fig 2.SEM images of a) CeO_2 and b) Palladium doped CeO_2

3.3. Energy Dispersive X-ray Analysis (EDAX)

The typical EDAX spectra of synthesized CeO_2 and Pd doped CO_2 catalyst is shown in Figure 3. In the synthesized CeO_2 and Pd dope, CO_2 catalysts having an atomic percentage of Ce and O were found to be 89.84 % and 10.16%, respectively. However, for the transition metal ion Pd^{2+}, doped CeO_2 nanoparticles, the atomic percentage of Ce, Pd, and O were found to be 82.24%, 0.18%, and 17.58%. The cerium percentage increased, and whereas the oxygen percentage also increased, this is due to the doping effects.

Table.2.Structural Parameter of $CeO_2$and $Ce_{0.98}Pd_{0.02}O_2$

Elements in CeO_2	**Weight (%)**	**Atomic (%)**	**Elements in Pd doped CeO_2**	**Weight (%)**	**Atomic (%)**
O K	10.16	49.77	O K	17.58	65.12
Ce L	89.84	50.23	Pd L	0.18	0.10
Totals	**100.00**	**100.00**	Ce L	82.24	34.78
			Totals	**100.00**	**100.00**

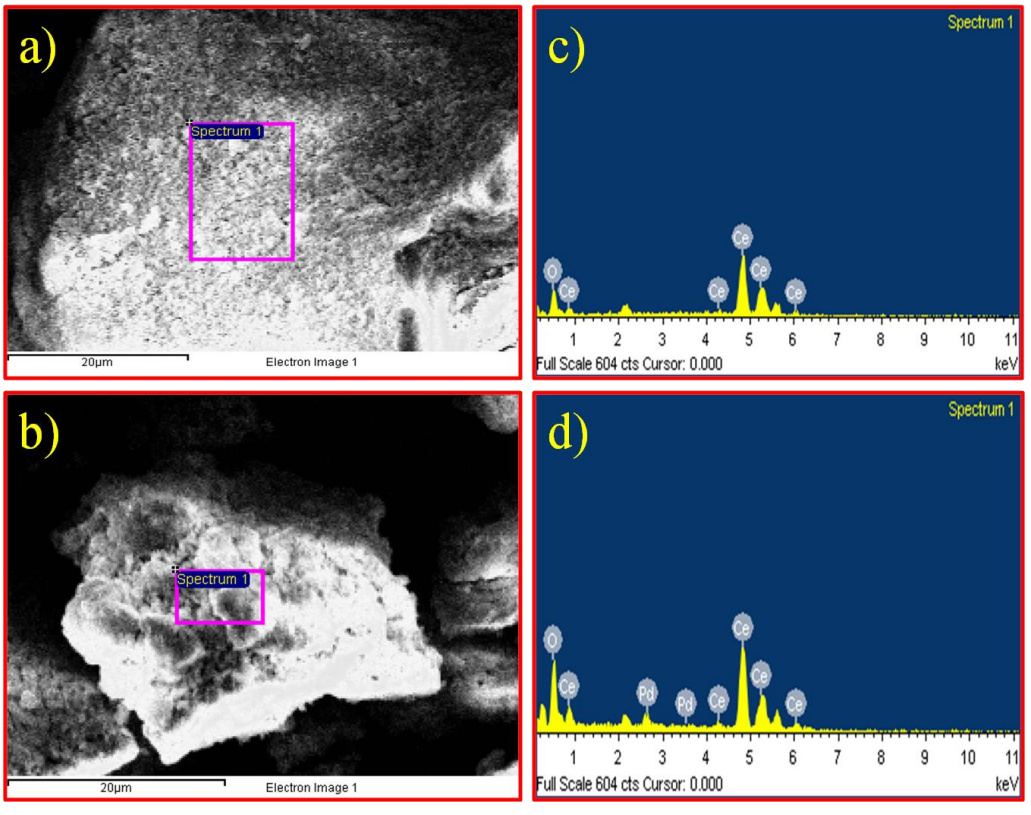

Figure 3. EDAX images of a) and c) CeO_2 and b) and d) Palladium doped CeO_2

3.4. FT-IR (Fourier Transformation-Infrared spectroscopic analysis)

The Fourier transformation-infrared spectra are used to recognize the functional group, study the vibration of atoms and molecules of CeO_2 and palladium doped CeO_2 shown in Fig. a) and b).Each Fourier transformation infrared spectra from Fig.a), it denotes 4-fold cerium coordination in vitreous matrix.3 absorbed peaks were discovered at 3426, 1622, and 1089. In Fig. b) showed vibration bands: 1622 cm^{-1} (HOH), 366 cm^{-1} correlation to Ce-O bond vibration, when increase temperature, the intensity vibration bands due to Ce-O bonds can increase the unit area made higher outlined. At a similar time, vibration band is present in water molecules, and structure can be diminished. The same profile is obtained for metal palladium doped CeO_2 as shown within the Fig.a).The synthesized FTIR spectrum of CeO_2 nanoparticles among the vary 500-4000 cm^{-1} that establish chemical bonds furthermore practical terms among the chemical element. The large, broadband showed at 3415 cm^{-1} is assigned due to the O-H vibration stretching in OH groups. The absorption peak around 1464 cm^{-1} is designated to the bending wave of C-H stretching. The critical band at 500 cm^{-1} corresponds to the Ce-O stretching vibrations [26, 27].

ISSN: 2005-4238 IJAST

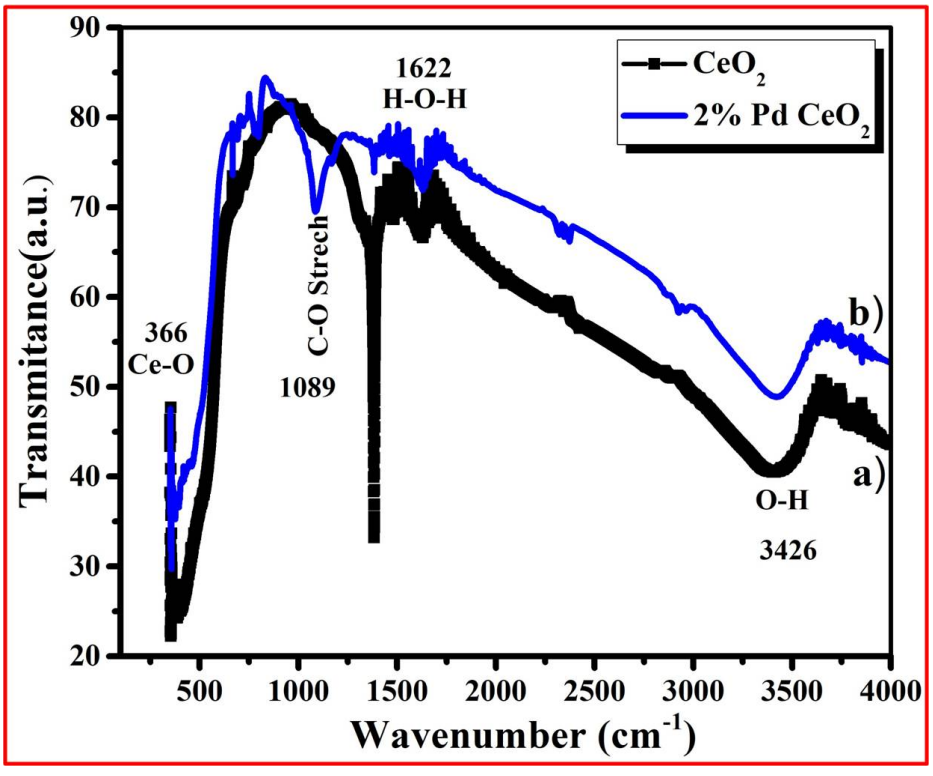

Fig.4. FTIR spectra of a) CeO_2 and b) Palladium doped CeO_2

3.5 X-ray photoelectron spectroscopy (XPS) studies

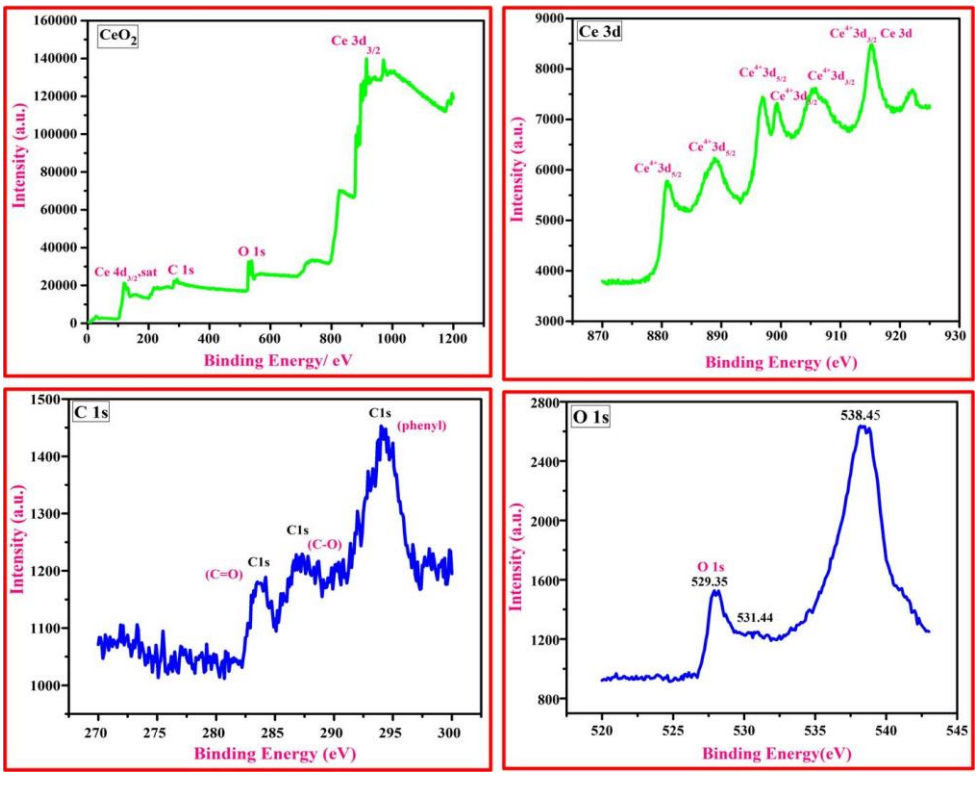

Fig.5. XPS images of CeO_2

The XPS analysis of CeO_2. Higher rates are observed due to Ce3d, Ce4d, O1, and C1. Fig. Shows how the Ce3d header is integrated into a different state, in addition to the XPS experimental data. The XPS of CeO_2 on the surface is shown to be two Ce3d and tetravalent Ce4d sulfur soils and can be solved with five $Ce3d^{5/2}$, $Ce3d^{3/2}$ spin-orbit double bonds [76, 77, 78-83]. Different levels of C1s were measured throughout the experiment; specifically, each XPS system observed increasing C1s levels at 285.07, 286, and 291.2 eV across all measurements and the combined power of all spectra averaged 285 eV for the C1s. We have investigated the oxidation states of Ce from high-grade O1s. O 1s deconvoluted spectra are shown in Fig 5. The bands added to the O1s show three thresholds at 530.5, 530.7, and 532.8 eV. The two mammals have higher frequencies at 530.5 eV and 530.7 eV respectively [76, 77, 84-86]. The third triplet peak at 532.8 eV has high oxygen/hydroxyl species similar to that reported in the present paper [87-89].

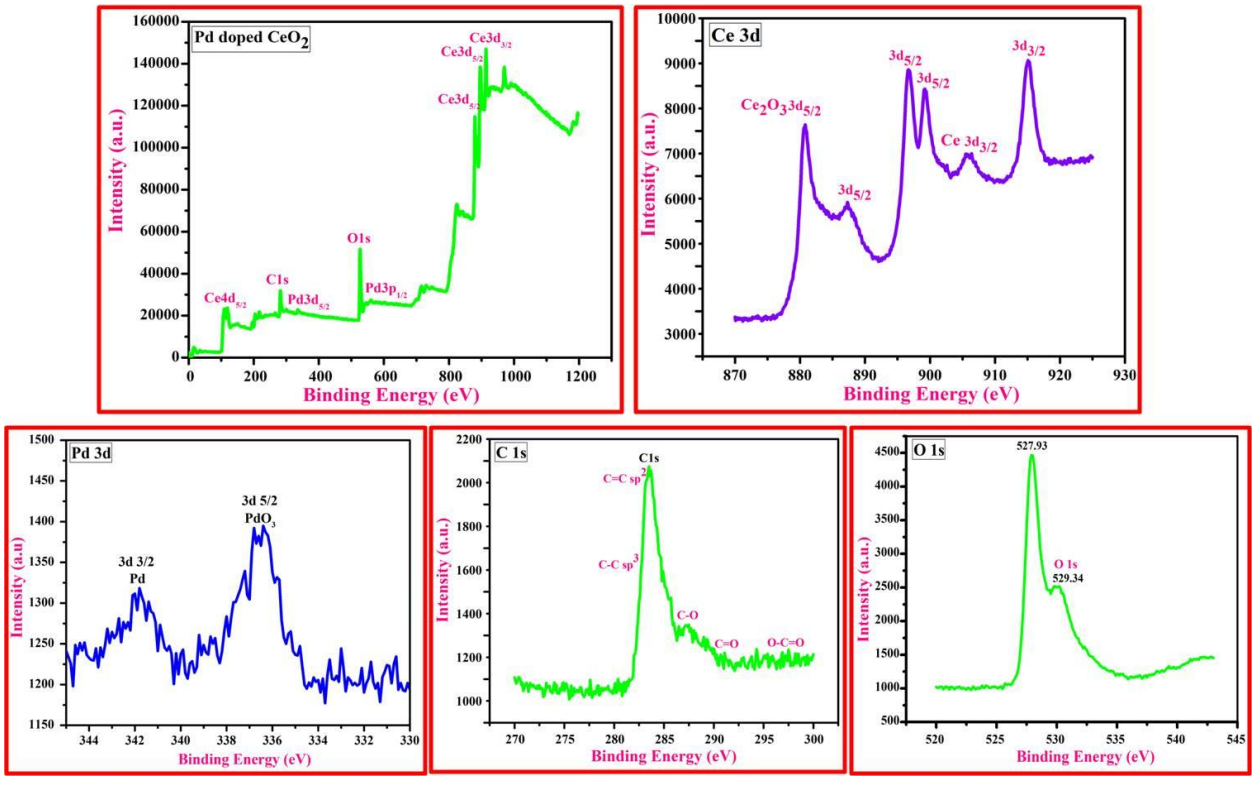

Fig.6. XPS images of Pd doped CeO_2

The XPS spectra of Pd doped CeO_2 were determined by measuring the concentrations of Ce3d, Pd3d, O 1s, and C 1s. XPS level Pd (3d) XPS was expressed in 2% Pd doped CeO_2 ($Ce_{0.98}Pd_{0.02}O_2$). Pd ($3d^{5/2}$) power was found to be correlated at 336.3 eV, which is higher than Pd^{2+} ($3d^{5/2}$) energy in association with PdO [90] but less than the potential of Pd^{2+} ($3d^{5/2}$) and 338 eV. and $PdCl_2$ [91]. So Pd is in 2+ state at ($Ce_{0.98}Pd_{0.02}O_2$). The X (3d) XPS levels are shown in the figure. From different levels of Ce (3d), we found that □10% Ce is in the 3+ state. Ce4d spectra of Ce4 show a two-dimensional peak with an energy of 896 and 912 eV. The presence of an additional peak at 887 eV and 905 eV is given to some Ce^{3+} ion activity related to oxygen generation [92]. These results demonstrate that the smoking states of Ce (IV) and Ce (III) are present in prepared preparations. The diagram is in fig. The Ce3d region is expressed by splitting the $Ce3d^{5/2}$ and $Ce3d^{3/2}$. The XPS of the Pd 3d region appears to be doubled at 336.3 eV, and 343.89 eV is the Pd^{2+} effect [93]. Another energy associated with 341.2 eV is related to Pd^0 $3d^{3/2}$, which also shows that the Pd elements are in the background. The low affinity for BE can be attributed to the relationship between palladium and cerium oxide in their analysis [94]. Due to the orbit coupling, Pd 3d films are divided into two $3d^{5/2}$ and $3d^{3/2}$ electrons, respectively. Two pairs of pegs were drawn and repeated, representing two Pd species. A couple may be more likely to be assigned to the Pd type, whereas a more stable couple may be

ISSN: 2005-4238 IJAST

present in the Pd (II) species. It is interesting to count on binding affinity for Pd species is higher compared to PdO or PdO [95]. In total, the Pd 3d level of the XPS shows that the absorbance energy of 336.4 eV is assigned to the Pd electron, and injected with the combined energy of 336.8 eV, corresponding to the PdO. The reflectance spectra of the O 1s show a similar peak in the potential energy (BE) of 529.9 eV of the oxygen atom in the cerium oxide. The presence of several O1s during the potential of 530 eV is due to the presence of oxide [96]. As shown in Figs. The O1s of the sample is divided into two groups. The peak at 530.9 eV is in the oxygen lattice, while the peak at 531.8 eV is chemisorbed oxygen [97]. In the C1s regions, the most affected signals were followed by sp^2 hybridization, with a BE of 285.97eV, follow by weak sp3, CeO, C-O, and O-C-O [98,99]. This signal is 283.49eV is air pollution [100]. The characteristic feature of the C1s region is the high potential C-C-sp^2 hybridization, and the coupling is 283.98eV.

3.6. UV-Visible absorption studies

The synthesized CeO_2 and Palladium doped CeO_2 were examined by UV-Visible spectro-photometer in Fig.3 Excellently-definite sharp-edged transmitted peak located at 329 nm. The transmitted peak moves toward the shorter wavelength to a higher wavelength. It indicates the slim, single particle size distribution obtained during this fabrication technique. Ultraviolet-Visible spectra showed no alternative peak connected with impurities and structural defects that confirmed that the synthesized nanoparticles square measure pure CeO_2. The absorption wavelength seems at concerning 329 nm for CeO_2 nanoparticles [29].The variation within the absorption peaks for comfortable and mixed chemical compound nanoparticles area unit because of the smaller size of nanoparticles [30].

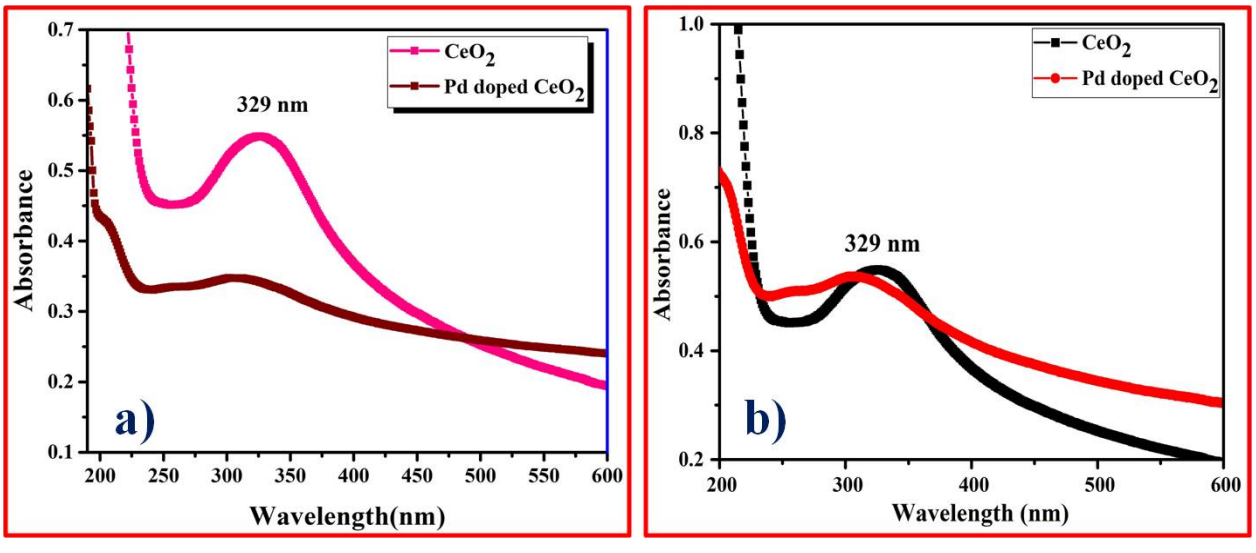

Fig.7. a) Solid UV-absorption spectra of a) CeO_2 and b) Palladium doped CeO_2, b) Liquid UV-absorption spectra of a) CeO_2 and b) Palladium doped CeO_2

4. Photocatalytic activities for the degradation of Congo red dye

Hydrophobicity of the gradient color in the presence of CeO_2 and Pd doped CeO_2 nanocomposite provides a lightening effect leading to changes in the concentration and duration of irradiation. (Fig.). Displays the optical fluctuations of the resulting CR fluorescence. It was found that irradiation of the presence of CeO_2 and Pd doped CeO_2 nanocomposite leads to a reduction in water content. Photoelectron spectra of CeO_2 and Pd doped CeO_2 were investigated, along with their performance comparison. It is found during the acceptance period that the amount of confirmation will decrease during the irradiation period. It showed that the absorption of the dye decreases in the presence of CeO_2 and that of the Nanoparticles of Pd doped CeO_2 under UV light. The red light at 497 nm (fig) decreased significantly during the irradiation period, with the restriction of the color ending within 120 min for CeO_2, while Pd doped CeO_2 exhibited

ISSN: 2005-4238 IJAST

degradation. The body lost at the end of 120 min, as seen in (fig). The peak was significantly worse during the irradiation period, indicating that a complete photoelectron had taken place to destroy the chromophore of the dye. Compared to the visible UV (sunlight) exposure of the red Congo colon, the photocatalytic ability of donors to damage red Congo significantly reduced extraction after irradiation. The experimental results concluded that the photocatalytic activity of CeO2 aggregates is much lower than that of Pd doped CeO_2, which indicates that Ce^{+4}, has a higher molecular weight than Pd^{2+}.

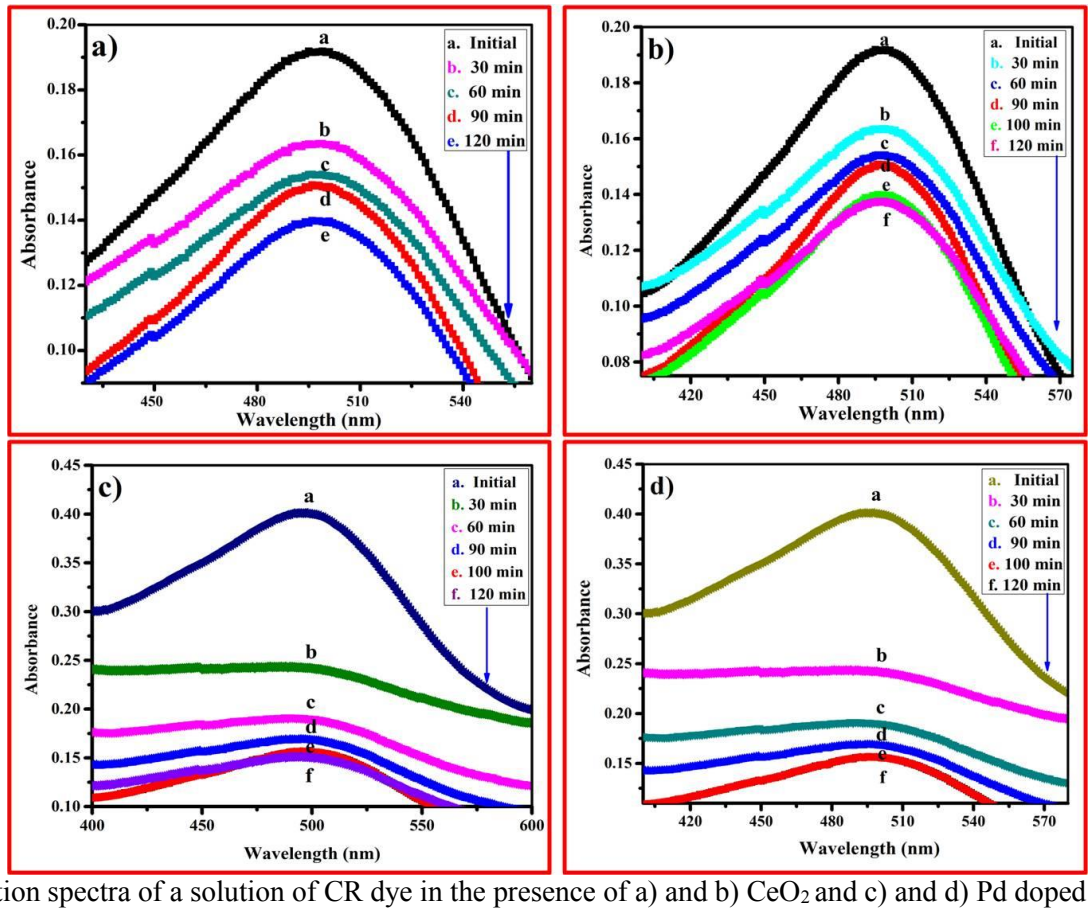

Fig. 8. Absorption spectra of a solution of CR dye in the presence of a) and b) CeO_2 and c) and d) Pd doped CeO_2 photocatalysts under exposure to UV light and visible light at different irradiation time intervals.

4.1 Photocatalytic activity by using UV-visible and Visible light (sunlight) irradiation

Photodegradation assay was performed on CR, a common antibiotic for UV irradiation in the photocatalytic experiments of CeO_2 and Pd doped CeO_2 To illustrate, the photodegradation of CR of CeO_2 and Pd doped CeO_2 in a non-catalytic manner was done. The photodegradation time course of the CR and the various inputs provide the experimental results shown in Figs. These results indicate that the CR system is stable under visible and UV irradiation without any bandwidth. When CeO_2 and Pd doped CeO_2 were added to the CR solution, the photocatalytic degradation rate of CeO_2 reached approximately 94% within 120 minutes of irradiation, less than that of Pd doped CeO_2 that could reach 86% of the total decomposition. Fig. Displays the destruction of the red-brown Congo of the sediments under the dark, presence, and presence of CeO_2 and Pd doped CeO_2. From the results, CeO_2 and Pd doped CeO_2 nanocomposite showed excellent photocatalytic activity due to the interaction effects of CeO_2 and Pd doped CeO_2 nanocomposite. CeO_2 unlocked showed 94%, with Pd doped CeO_2 catalyst shows 86% of degradation Congo red of water is cooled after 122 min. At the same time, no photodegradation was observed in the absence of an analyte. The result revealed that CeO_2 nanocomposite exhibited unusual photocatalytic activity for hair follicles.

ISSN: 2005-4238 IJAST

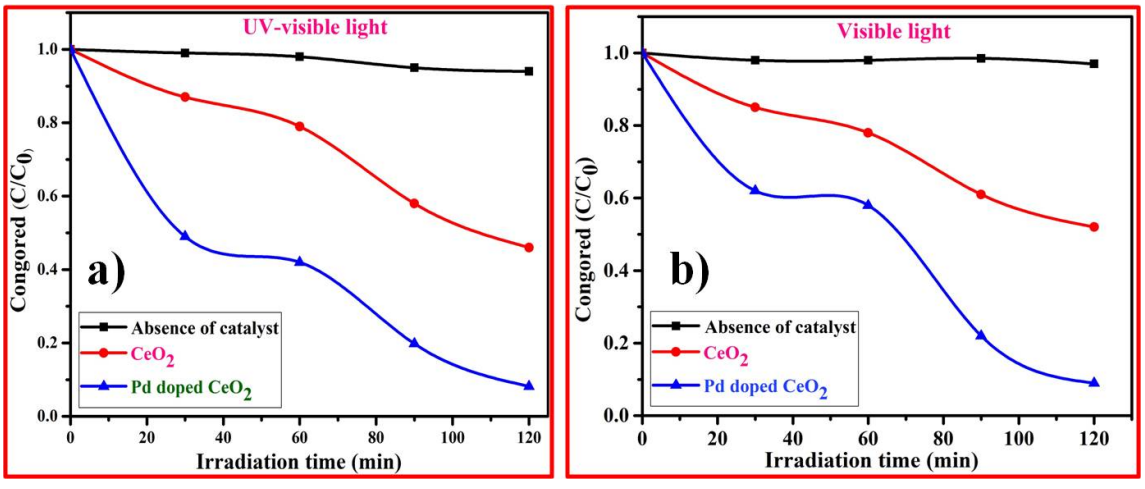

Fig. 9. (a) The photocatalytic degradation of CR dye in absence and presence over different photocatalysts under visible light and UV-visible light irradiation.

4.2 Degradation percentages (%) of Congo red dye and E□ect of di□erent nature of light sources on photocatalytic activity

Contribution of Congo red and reddened CeO_2 to Pd doped CeO_2. To evaluate the characteristics of the suppliers, the degradation rate of the red dye was calculated in Table 1. It is, therefore, excluded from the study that CeO_2 effluent was found to be better than Pd doped CeO_2. The pure act was obtained by quantifying Congolese and red color images using CeO_2 and Pd doped CeO_2 NPS. The two most common types of lighting are sun and UV-light. The experiments were performed by diffusing 60mg of CeO_2 and Pd doped CeO_2 Nps in 100ml of red pepper extract of 20ppm Congo. The photocatalytic degradations of Congo red for 120 min are higher in UV light (93%) than in sunlight (85%). This is because the UV light is high (low waves or high energy), so light can penetrate rapidly and result in a large number of radicals, which increase in the rate of photocatalytic damage of Congo red.

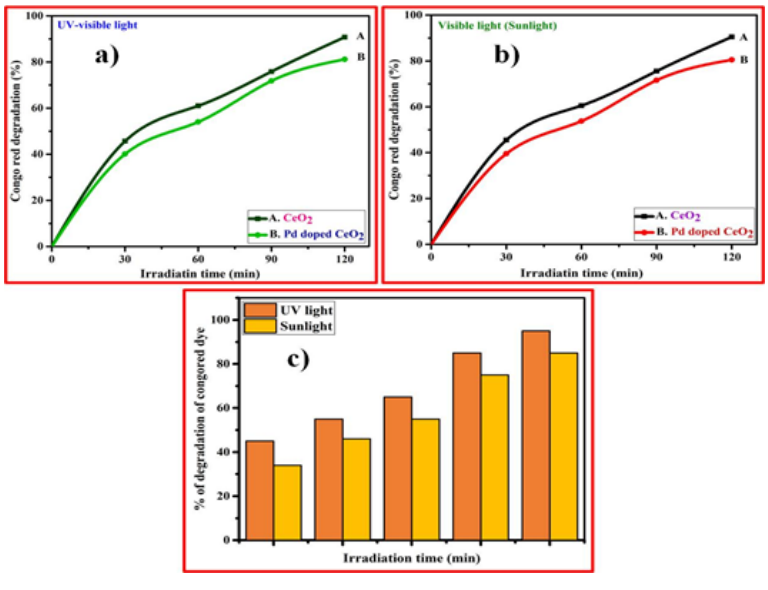

Fig.10. Degradation percentages (%) of Congo red dye using UV light and Sunlight by using the photocatalysts (a) CeO_2 and (b) Pd doped CeO_2 nanoparticles.

4.3 Comparative study of the e□ects of di□erent source of light on photocatalytic activity using

different CeO_2 and Pd doped CeO_2 nanoparticles and Degradation percentage (%) of Congo red dye by the use of CeO_2 and Pd doped CeO_2 catalyst

No.	Light sources	Catalysts	Weight of catalysts	Dye concentration	Degradation time	Degradation (%)
1	**UV-light**	CeO_2	60 mg	20 ppm	120 min	94
2	**Sunlight**	$Ce_{0.98}Pd_{0.02}O_2$	60 mg	20 ppm	120 min	86

4.4 Effects of catalyst weight

The catalyst quantities for CR dye in 20 ppm were 60 mg, Reduction of dose increases with supplier rate and indicates significant reductions in doses of up to 60 mg; This might be too several potent sites present when the load is 60 mg, which increases in photons, resulting in increased photodegradation. Behind the level results in no significant change observed in photodegradation because the problem of annealing increases with increasing concentration leading to a reduction in light intensity and a reduction in photodegradation.

4.5 Effects of initial dye concentrations

The results of the first CR were evaluated on the efficiency of photodegradation by a concentration of 20 ppm. The decrease in photoluminescence after daylight is 20 ppm, and when that is reduced, this is due to the inhibition of photocatalyst active sites and reduced photon interactions at these sites. The increased concentration of hair follicles leads to an increase in the use of artificial insemination in photos. However, the reduction of photocatalytic degradations is due to the low levels of oxygen produced by the sun. On the other hand, increasing the intensity of hair loss, the photodegradation efficiency decreased, so that fewer sites were active in the sample, and as a result, photodegradation efficiency decreased.

4.6 Reusability

Persistence and ability to engage are essential for their practical application. The sample was determined by repeating a five-photon photodegradation experiment of the same method, and the results of this model are shown. The acquisition results showed a slight decrease in photodegradation performance at each time point and no distortion that resulted in the completion of the fifth phase, which showed the positive energy of the analyst. The reconstitution of CeO_2 nanocatalyst is investigated by the degradation process of staining; The activities of the reactor decreased gradually during the fifth 90 after 90, and this may be due to the removal of the ion from the upper particle. The screwdriver separates and recovers when the centrifuge responds. CeO_2 nanocatalysts that are recovered due to oxidative damage can be resumed. The percentage of loss was nearly equal for the first three episodes, and it began to decline slightly in the fourth series, and that may have been due to management control during the recovery process. At 95% (presence of CeO_2 nanocatalysts) for CR and 55.02% (presence of Pd doped CeO_2 nanocatalysts) for CR of the staining ended after 100 and 90 min, respectively. It can be inferred that the percentage of degradations of nutrients from CeO_2 nanocatalysts is high than Pd doped CeO_2. The above results demonstrate that the complementary CeO_2 nanocube exhibit excellent photocatalytic activity, which may be due to the unique properties of CeO_2. Our CeO_2 mixtures play a significant role and show good exercise for the destruction of the toxin.

Mechanism as follows:-

$$CeO_2 \text{ visiblelight} \rightarrow CeO_2(e^- + h^+) \qquad (1)$$

ISSN: 2005-4238 IJAST

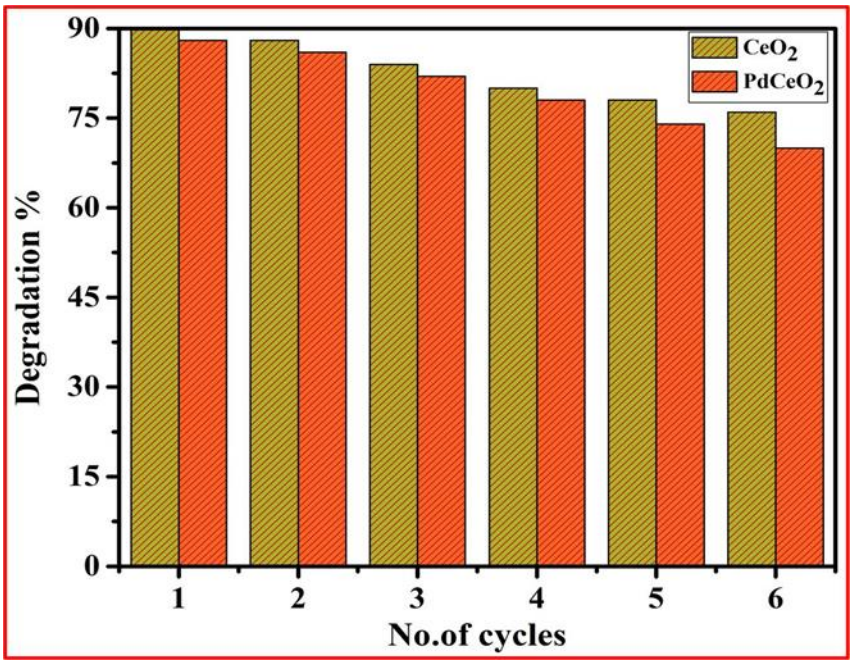

Fig 11. Recyclable properties of Congo red dye by using CeO_2 and Pd doped CeO_2 catalysts

3. Conclusion

From the PXRD discovered the standard crystalline size of CeO_2, $Ce_{0.98}Pd_{0.02}O_2$ catalysts were obtained at 5.9 nm and 3.1nm. The synthesized nanoparticles having polygonal shape structure; this structure showed that the $Ce_{0.98}Pd_{0.02}O_2$ catalyst doesn't change morphology. The FTIR structure exhibited the presence of Ce-O stretching bonds of CeO_2. The CeO_2 nanoparticles showed powerful UV-visible absorption at 329 nm with bandgap was resolution relating 3.26 eV, the polygonal shape morphology with uniform distribution of particles. In Fig.a) and b).The SEM analysis showed morphology CeO_2 and $Ce_{0.98}Pd_{0.02}O_2$. The $Ce_{0.98}Pd_{0.02}O_2$ catalyst doesn't affect the morphology and arrangement of the CeO_2 nanoparticles. This reveals the $Ce_{0.98}Pd_{0.02}O_2$ was a critical application for element oxygen storage capability, element uptake measurements, CO reaction studies, and reduction catalyst in coupling reactions. The pure act was obtained by quantifying Congolese and red color images using CeO_2 and Pd doped CeO_2 NPS. The two most common types of lighting are sun and UV-light. The experiment was performed by spreading 60mg of CeO_2 and Pd doped CeO_2 Nps in 100ml of red pepper extract of 20ppm Congo. From Table one, it can be observed that the photocatalytic degradations of Congo red for 120 min is higher in UV light (93%) than in sunlight (85%). This is because the UV light has high energy (low waves or high energy), so that light can penetrate rapidly and produce large quantities of free radicals, which increase the rate of photocatalytic destruction of Congolese red dye.

Acknowledgments

The one of the author (G.O. Obaiah) thanks to the University grants commission (UGC), New Delhi and National Fellowship for Higher education (NFST) award letter no F.17.1/2015-16/ NFST -2015-17-ST-KAR-2348/(cpp- II), dated 11-01-2013 for the finance assistance to complete the research work.

The one of the author (G.O. Obaiah) thank to the Research center, Talent development center, IISC, Kudhapur, Chitradurga, providing the lab facilities for completion of the work.

References:

[1]. Darroudi M, Sarani M, et al., (2014) Ceram. Int. 40:2863-2868.
[2]. Devaraja P B, Avadhani D N, Prashanthaet al,(2014) Spectrochim. Acta Part A.121:46-52.
[3]. Dhananjaya N, Nagabhushana H, Nagabhushana B, et al., (2012) Spectrochim. Acta Part A.96:532-540.
[4]. Negishi E, (2000) Wiley, Chichester. The UK.
[5]. Tsuji J, John Wiley & Sons, Ltd, Chichester, UK, 2004.
[6]. Willner, Maidan R, Mandler D, Durr H, Dorr G, Zengerle K, Am J. Chem. Soc. 1987, 109, 6080.
[7]. Mizukoshi Y, Okitsu K, Maeda Y, Yamamoto T A, Oshima R, Nagata Y, Phys J. Chem. B. 1997, 101,7033.
[8]. Qin Y H, Yang HH, Zhang X S, Li P, Ma C A, Int. Hydrog J. Energy. 2010, 35, 7667-7674.
[9]. Zhang Z, Liu J, Gu J, Su L, Cheng L, Energy Environ. Sci. 2014, 7 2535-2558.
[10]. Shido T, Iwasawa Y, Catal J. 141 (1993) 71.
[11]. BunluesinT, Gorte R J and GrahammG W, Appl. Catal. B: Environ., 15 107 (1998)
[12]. Xc C and Kang P, Shen, Chem. Commun.,2238 (2004)
[13]. Xc C and Kang P, Shen, Chem. Commun.,2238 (2004)
[14]. Mogensen, N, Sammes M, and Tompsett G A, Solid State Ionics, 129, 63 (2000)
[15]. Wang Z L, and Feng X D, Phys J. Chem. B,107,13563 (2003)
[16]. Miki T, Ogawa T, Haneda M, Kakuta N, (1990) Phys J. Chem., 94:6464.
[17]. Qin Y H, Yang HH, Zhang X S, Li P, Ma C A, Int. Hydrog J. Energy. 2010, 35, 7667-7674.
[18]. Zhang, J, Liu J, Gu, Su L, Cheng L, Energy Environ. Sci. 2014, 7 2535-2558.
[19]. ShidoY, Iwasawa J, Catal. 141 (1993) 71.
[20]. Bunluesin, Gorte R J and Grahame GW, Appl. Catal. B: Environ., 15 107 (1998)
[21]. XcCand Kang P, Shen, Chem. Commun.,2238 (2004)
[22]. ZhangC, XuL, Shan N, Sun T, Chem J, Yan Y, ACS Catal. 2014, 1926-1930.
[23]. Shao Y, Sui J, Yin G, Gao Y, Appl. Catal. B-Environ. 2008, 79, 89-99.
[24]. Yoldas B E, O'Keeffe T W, Appl. Opt. 1979, 18, 3133-3138.
[25]. Ranjit KT, Varadarajan T K, Viswanathan B, Photochem J. Photobiol. A Chem. 1996, 96A 18-185.
[26]. Zhang Z, Kleinstreuer C, Donohue J F, and Kim C S, Aerosol Sci.J 36 (2005)
[27]. McDevitt T and Baun W L, Spectrochimica Acta 20 (1964) 799-808
[28]. Rema Devi BS, Raveendran Rand Av Vaidyan. Pramana –J.Physics Vol.68, No.4, April(2007) 679687
[29]. change,et al,Appl.phys.Lett 80 ,(2002) 127.
[30]. Obaiah G O, Shivaprasad K H, Mylarappa M, et al., (2018) Advanced Science Letters.24: 6004-6007(4)
[31]. Obaiah G O, Shivaprasad K H, Mylarappa M, et al.,(2018) Materials Today: Proceedings 5:22466–22472.
[32]. K. Maeda, K. Domen, Photocatalytic properties of RuO_2-loaded b-Ge_3N_4 for overall water splitting, J. Phys. Chem. C 111 (12) (2007) 4749–4755.
[33]. Y. Inoue, Photocatalytic water splitting by RuO_2-loaded metal oxides and nitrides with d^0- and d^{10}-related electronic configurations, Energy Environ. Sci. 2 (4) (2009) 364–386.
[34]. A. Kudo, Y. Miseki, Heterogeneous photocatalyst materials for water splitting, Chem. Soc. Revis. 38 (1) (2009) 253–278.
[35]. T.J. Fisher, M. Wang, Y. Ibrahim, B. Steffensmeier, C.L. Cheung, Effect of sodium nitrate on the microwave-assisted synthesis of ceria nanocubes, Mater. Lett., 178 (2016) 71-74.
[36]. A. Primo, T. Marino, A. Corma, R. Molinari, H. Garcia, Efficient visible-light photocatalytic water splitting by minute amounts of gold supported on nanoparticulate CeO2 obtained by a biopolymer templating method, J. Am. Chem. Soc., 133(18) (2011) 6930-6933.

[37]. Magesh, G., Viswanathan, B., Viswanath, R. P. & Varadarajan, T. K. Photocatalytic behavior of CeO2-TiO2 system for the degradation of methylene blue. Indian J. Chem. B Org. 3, 480–488 (2009).
[38]. Truffault, L. et al. Application of nanostructured Ca doped CeO2 for ultraviolet filtration. Mater. Res. Bull. 45, 527–535 (2010).
[39]. V. Addorisio, S. Esposito and F. Sannino, Sorption Capacity of Mesoporous Metal Oxides for the Removal of MCPA from Polluted Waters, J. Agric. Food Chem., 2010, 58, 5011–5016.
[40]. A.K. Aboul-Gheit, D.S. El-Desouki, R.A. El-Salamony, Different outlet for preparing nano-TiO_2 catalysts for the photodegradation of Black B dye in water, Egypt. J. Inst. Pet. 23 (2014) 339–348.
[41]. W. Shen, Z. Li, H. Wang, Y. Liu, Q. Guo, Y. Zhang, Photocatalytic degradation for methylene blue using zinc oxide prepared by co-deposition and sol-gel methods, J. Hazard Mater. 152 (2008) 172–175.
[42]. S.W. Kim, H.-K. Kim, H.W. Choi, D.-H. Yoo, E.J. Kim, S.H. Hahn, Photocatalytic activity of metal-inserted WO, Nanosci. Nanotechnol. 13 (2013) 7053–7055.
[43]. R.G. Toro, G. Malandrino, I.L. Fragala, R. Lo Nigro, M. Losurdo, G. Bruno, Relationship between the nanostructures and the optical properties of CeO_2 thin films, J. Phys. Chem. B 108 (2004) 16357–16364.
[44]. S. Kanakaraju, S. Mohan, A.K. Sood, Optical and structural properties of reactive ion beam sputter deposited CeO_2 films, Thin Solid Films 305 (1997) 191–195.
[45]. C.s.O. Avellaneda, M.A.C. Berton, L.O.S. Bulhoes, Optical and electrochemical properties of CeO_2 thin film prepared by an alkoxide route, Sol. Energy Mater. Sol. Cell. 92 (2008) 240–244.
[46]. D. Channei, B. Inceesungvorn, N. Wetchakun, S. Ukritnukun, A. Nattestad, J. Chen, S. Phanichphant, Photocatalytic degradation of methyl orange by CeO2 and Fe–doped CeO2 films under visible light irradiation, Sci. Rep. 4 (2014) 1–7.
[47]. A. Akbari–Fakhrabadi, R. Saravanan, M. Jamshidijam, R.V. Mangalaraja, M.A. Gracia, Preparation of nanosized yttrium doped CeO2 catalyst used for the photocatalytic application, J. Saudi Chem. Soc. 19 (2015) 505–510.
[48]. N. Sabari Arul, D. Mangalaraj, T. Whan Kim, P. Chi Chen, N. Ponpandian, P. Meena, Y. Masuda, Synthesis of CeO2 nanorods with improved photocatalytic activity: Comparison between precipitation and hydrothermal process, J. Mater. Sci-Matter. El. 24 (2013) 1844–1650.
[49]. S. Jayapalan, K.S. Ranjith, S. Padmanapan, D. Mangalaraj, R.T. Rajendrakumar, Cobalt–doped cerium oxide nanoparticles: Enhanced photocatalytic activity under UV and visible light irradiation, Mat. Sci. Semicon. Proc. 26 (2014) 218–224.
[50]. L. Truffault, Application of nanostructured Ca doped CeO2 for ultraviolet filtration, Mater. Res. Bull. 45 (2010) 527–535.
[51]. J.M.A. Almeida, P.E.C. Santos, L.P. Cardoso, C.T. Meneses, A simple method to obtain Fe–doped CeO2 nanocrystals at room temperature, J. Magn. Magn. Mater. 327 (2013) 185–188.
[52]. S. Ye, K. Ullah, L. Zhu, Z.D. Meng, Q. Sun, W.C. Oh, Easy and Fast Synthesis of Pd–MWCNT/TiO2 by the Sol-Gel Method and its recycling photodegradation of rhodamine BJ. Korean Ceram. Soc. 50 (2013) 251–256.
[53]. S.A. Ansari, M.M Khan, M.O. Ansari, S.Kalathil, J.Lee, M.H. Cho, Band Gap Engineering of CeO2 Nanostructure by Electrochemically Active Biofilm for Visible Light Applications, RSC Adv. 4 (2014) 16782-16791.
[54]. W. Deng, D. Chen, J. Hu, and L. Chen, A general and green approach to synthesize monodisperse ceria hollow spheres with enhanced photocatalytic activity, RSC Adv. 5 (2015) 80158-80169
[55]. A. Umar, R. Kumar, M.S. Akhtar, G. Kumar, S.H. Kim, Growth and properties of Well-crystalline cerium oxide nanoflakes for environmental and sensor applications, J.Colloid.Interf.Sci. 454 (2015) 61–68

[56]. S. Ansari, M. Khan, M.O. Ansari, S. Kalathil, J. Lee1, and M.H. Cho, Band Gap Engineering of CeO2 Nanostructure by Electrochemical Active Biofilm for Visible Light Applications, RSC Adv. 4 (2014) 16782-16791
[57]. J. Ko, J.H. Kim, and C.B. Park, Synthesis of visible light-active CeO2 sheets via mussel-inspired CaCO3 mineralization, J. Mater. Chem. A, 2013, 1,241
[58]. C. Mao, Y. Zhao, X. Qiu, J. Zhu, and C. Burda, Synthesis, characterization and computational study of nitrogen-doped CeO2 nanoparticles with visible-light activity, Phys. Chem. Chem. Phys. 10 (2008) 5633–5638.
[59]. G. Zhang, J. Ao, Y. Guo, Z. Zhang, M. Shao, L. Wang, L. Zhou and J. Shao, Green synthesis and catalytic performance of nanoscale CeO2 sheets, RSC Adv.4 (2014) 20131-20135
[60]. Y. Li, Q. Sun, M. Kong, W. Shi, J. Huang, J. Tang, X. Zhao, J. Phys. Chem. C 115 (2011) 14050–14057.
[61]. A.D. Liyanage, S.D. Perera, K. Tan, Y. Chabal, K.J. Balkus Jr, ACS Catal. 4 (2) (2014) 577–584.
[62]. S.A. Ansari, M.M. Khan, M.O. Ansari, S. Kalathil, J. Lee, M.H. Cho, RSC Adv. 4 (2014) 16782–16791.
[63]. D. Channei, B. Inceesungvorn, N. Wetchakun, S. Phanichphant, A. Nakaruk, P. Koshy, C.C. Sorrell, Photocatalytic activity under visible light of Fe-doped CeO2 nanoparticles synthesized by flame spray pyrolysis, Ceram. Int. 39 (2013) 3129–3134.
[64]. S. Mansingh, D.K. Padhi, K.M. Parida, Enhanced photocatalytic activity of nanostructured Fe doped CeO2 for hydrogen production under visible light irradiation, Int. J. Hydrogen Energy. 41 (2016) 14133–14146.
[65]. P.Li, W. Zhang, X.Zhang, Z. Wang, X.Wang, S. Ran, Y. Lv, Synthesis, characterization, and photocatalytic properties of flower-like Mn-doped ceria, Mat. Res. 21 (2018) 1–6.
[66]. S. Mansingh, D.K. Padhi, K.M. Parida, Enhanced photocatalytic activity of nanostructured Fe doped CeO2 for hydrogen production under visible light irradiation, Int. J. Hydrogen Energy. 41 (2016) 14133–14146.
[67]. P.Li, W. Zhang, X.Zhang, Z. Wang, X.Wang, S. Ran, Y. Lv, Synthesis, characterization, and photocatalytic properties of flower-like Mn-doped ceria, Mat. Res. 21 (2018) 1–6.
[68]. V. Binas, D. Venieri, D. Kotzias, G. Kiriakidis, Modified TiO2 based photocatalysts for improved air and health quality, J. Materiomics. 3 (2017) 3–16.
[69]. D. Channei, S. Phanichphant, A. Nakaruk, S.S. Mofarah, P. Koshy, C.C. Sorrell, Aqueous, and surface chemistries of photocatalytic Fe–doped CeO2 nanoparticles, Catal. 45 (2017) 1–23.
[70]. M. Zhang, X. Yu, D. Lu, J. Yang, Facile synthesis, and enhanced visible-light photocatalytic activity of N and Zr co-doped TiO2 nanostructures from nanotubular titanic acid precursors. Nanoscale Research Letters. 8 (2013) 543–552.
[71]. L. Yue, X.M. Zhang, Structural characterization and photocatalytic behaviors of doped CeO_2 nanoparticles, J. Alloys Compd. 475 (2009) 702-705.
[72]. D. Ma, Y. Zhao, J. Zhao, Y. Li, Y. Lu, D. Zhao, Aqueous synthesis of hierarchical bismuth nanobundles with high catalytic activity to organic dyes, Superlattice. Microsoft. 83 (2015) 411–421.
[73]. K.H. Kim, S.K. Ihm, Heterogeneous catalytic wet air oxidation of refractory organic pollutants in industrial wastewaters: a review, J. Hazard. Mater. 186 (2011) 16–34.
[74]. P. Ji, J. Zhang, F. Chen, M. Anpo, Study of adsorption and degradation of acid orange seven on the surface of CeO_2 under visible light irradiation, Appl. Catal. B: 484, Environ. 85 (2009) 148–154.
[75]. B. Subash, B. Krishnakumar, R. Velmurugan, M. Swaminathan, M. Shanthi, Synthesis of Ce co-doped Ag–ZnO photocatalyst with excellent performance for NBB dye degradation under natural sunlight illumination, Catal. Sci. 488 Technol. 2 (2012) 2319–2326.
[76] Rema Devi B S, Raveendran Rand Av Vaidyan. Pramana –J.Physics Vol.68, No.4, April(2007) 679687
[77] ZhangF,et al,Appl.phys.Lett 80 ,(2002) 127.

[78] E.J. Preisler, O.J. Marsh, R.A. Beach, T.C. McGill, J. Vac., Sci. Technol. B 19 (2001) 1611.
[79] V. Fernandes, I.L. Graff, J. Varald, L. Amaral, P. Fichtner, D. Demaille, Y. Zheng, W.H. Schreiner, D.H. Mosca, J. Electrochem. Soc. 159 (2012) K27.
[80] D.R. Mullins, S.H. Overbury, D.R. Huntley, Sur. Sci. 409 (1998) 307.
[81] V. Chauvaut, V. Albin, H. Schneider, M. Cassir, H. Ardelean, A. Galtayries, J. Appl. Electrochem 30 (2000) 1405.
[82] E. Beche, P. Charvin, D. Perarnau, S. Abanades, G. Flamant, Sur. Inter. Anal. 40, (2008) 264. [83] Y. Zhou, J.M. Perket, J. Zhou, J. Phys. Chem. C 114 (2010) 11853.
[84] F. Pagliuca, P. Luches, S. Valeri, Sur. Sci. 607 (2013) 164.
[85] B. Hirschauer, M. Gothelid, E. Janin, H. Lu, U.O. Karlsson, Appl. Sur. Sci. 148 (1999) 164.
[86] C.G. Kim, J. Vac., Sci. Technol. B 18 (2000) 2650.
[87] M.A. Henderson, C.L. Perkins, M.H. Engelhard, S. Thevuthasan, C.H.F. Peden, Surf. Sci. 526 (2003) 1.
[88] M.B. Hugenschmidt, L. Gamble, C.T. Campbell, Surf. Sci. 302 (1994) 329.
[89] Y. Lykhach, V. Johanek, H.A. Aleksandrov, S.M. Kozlov, M. Happel, T. Skala, P. StPetkov, N. Tsud, G.N. Vayssilov, K.C. Prince, K.M. Neyman, V. Matolin, J. Libuda, J. Phys. Chem. C 116 (2012) 12103.
[90]. M. Brun, A. Berthet, and J. C Bertolini, J. Electron Spectrosc. Relat. Phenom., 104, 55 (1999)
[91]. T. Baidya, A. Gupta, P. A. Deshpande, G. Madras, and M. S. Hegde, J. Phys. Chem. C, 113, 4059 (2009).
[92] C. Zhang, J. Lin, Visible-light induced oxo-bridged ZrIV-O-CeIII redox Centre in tetragonal ZrO2-CeO2 solid solution for degradation of organic pollutants, Phys. Chem. Chem. Phys. 13 (2011) 3896–3905.
[93] Q. Zhang, X. Wu, M. Gao, H. Qiu, J. Hu, K. Huang, S. Feng, Y. Yang, T. Wang, B. Zhao, Z. Liu, Highly active electrocatalyst of 3D Pd/reduced graphene oxide nanostructure for electro-oxidation of methanol and ethanol, Inorg. Chem. Commun. 94 (2018) 43–47.
[94] M. Peuckert, XPS study on the surface and bulk palladium oxide, its thermal stability, and a comparison with other noble metal oxides, J. Phys. Chem. 89 (12) (1985) 2481–2486.
[95] C.D. Wagner, W.M. Riggs, L.E. Davis, J.F. Moulder, G.E. Muilenberg, Handbook of X-Ray Photoelectron Spectroscopy, Perkin-Elmer Corporation, Eden Prairie, Minnesota, 1979, p. 111 (In Anonymous).
[96] M. Wang, D. Fang, N. Wang, S. Jiang, J. Nie, Q. Yu, G. Ma, Preparation of PVDF/ PVP core-shell nanofibers mats via homogeneous electrospinning, Polymer 55 (2014) 2188–2196.
[97] W. Zhang, Q. Zhang, B. Yu, L. Zhao, Quality & Quantity 49 (2015) 1023-1038. [98] J.Cao, L.Song, J.Tang, J.Xu, W.Wang, Z.Chen, Appl.Surf.Sci.274(2013) 138–143.
[99]A.A.Siller-Ceniceros, M.E.Sánchez-Castro, D.Morales-Acosta,J.R.Torres-Lubian, E.G.Martínez,F.J.Rodríguez-Varela,Appl.Catal.BEnviron.209(2017)455–467.
[100] S.M.SenthilKumar,J.SolerHerrero, S.Irusta, K.Scott, J.Electroanal.Chem.647 (2010)211–221.

ISSN: 2005-4238 IJAST